TORSIONAL MODAL DAMPING OF A LCI DRIVEN GEARED
MOTO-COMPRESSOR TRAIN: EVALUATION, OPTIMIZATION CRITERIA AND ACTIVE CONTROL

Gaspare Maragioglio
Engineering Manager
Power Transmission
GE Oil & Gas
Florence, Italy
gaspare.maragioglio@ge.com

Daniele Sgrò
Senior Engineer
Electrical System Engineering
GE Oil & Gas
Florence, Italy
daniele.sgro@ge.com

Paolo Calore
Lead Engineer
Advanced Train Integration
GE Oil & Gas
Florence, Italy
paolo.calore@ge.com

Lorenzo Failla
Lead Design Engineer
Advanced Train Integration
GE Oil & Gas
Florence, Italy
lorenzo.failla@ge.com

Pierluigi Tenca
Senior Engineer, PhD
Electrical Technologies
GE Global Research Center
Munich, Germany
pierluigi.tenca@ge.com

Gaspare Maragioglio is currently Engineering Leader of Power Transmission for GE Oil & Gas, in Florence, Italy. He is responsible for technical selection of flexible/rigid couplings, auxiliary equipment and gears design, with particular focus on the train rotor-dynamic behavior, torsional and lateral. He has a degree in Mechanical Engineering and before joining GE he had a research assignment at University College London. He is currently member of API613 Task Force and the ATPS Advisor Committee.

Daniele Sgrò is currently working as Senior Electrical System Engineer at GE Oil & Gas, Florence, Italy. His main areas of expertise are related to the electro-mechanical system design of rotating electrical machines, involving motor-compressor, turbo-generator and LNG applications. He co-authored some publications at International Conferences for the Oil & Gas Industry. He received the M.Sc. Degree in Mechanical Engineering with major in Mechatronics from the Polytechnic of Milan, Italy in 2009.

Paolo Calore is currently working as Lead Rotor and Structural Dynamics Engineer at GE Oil & Gas, Florence, Italy. In the past, he used to work as Stress Engineer for Engine Dynamics at AIRBUS, on behalf of Safran Group, in Toulouse, France. His main interests are rotor dynamics, FE modelling and structures' damping. He co-authored a publication in Mechanical Systems and Signal Processing (Elsevier). He took a B.Sc. in Aerospace Engineering and a M.Sc. in Aeronautical Engineering with a major in structural dynamics from Sapienza, University of Rome (Italy) in 2012.

Lorenzo Failla is currently working as Lead Shaft Line Design Engineer at GE Oil & Gas, Florence, Italy. In the past, He used to work as System Engineer for HVAC Systems at AnsaldoBreda, Italy. His main interests are rotor dynamics test bench data analysis, analysis automation and software development. He took a M.Sc. in Mechanical Engineering with a major in industrial automation from University of Florence (Italy) in 2005.

Pierluigi Tenca is currently working as Senior Research Engineer at GE Global Research Center (GRC), Munich, Germany on High Power Electronics and Motor Drives topics. He received the M.Sc. in Signal and Communication Electronics, as well as the Ph.D. in High Power Electronics from the University of Genova, Italy, in 1996 and 2000. He spent part of his Ph.D. in the Dept. of Electronic and Electrical Eng., Univ. of Bath, U.K. From 2000 to 2003 he was R&D Engineer in Siemens Transportation Systems, Erlangen, Germany working on Converters for High Power Locomotives. From 2003 to 2005 he was Post-Doc Researcher with Prof. Thomas Lipo at WEMPEC, Univ. WI Madison, USA. From 2005 to 2008, he worked in Ansaldo Sistemi Industriali on the joint development, commissioning and field testing of 35MW modular MV motor drive clusters with GE Oil & Gas and GRC. From 2008 to 2013, he worked in ABB Corporate Research Center, Västeras, Sweden on motors identification and control, metrology techniques and, mainly, modular multilevel topologies for HVDC Transmission. He received two IEEE Paper Awards, authored or coauthored more than 40 papers and Patent

ABSTRACT

The torsional modal response of geared compression trains driven by Variable Speed Drive Systems (VSDS) can be heavily affected by electro-mechanical interaction phenomena, both in terms of excitation mechanism and resulting damping contribution. A thorough understanding of these phenomena is essential to optimize the system design of motor-compressor shaft lines, thus avoiding equipment oversizing and minimizing string tests and commissioning time.

This paper provides a comprehensive analysis of the key systems and parameters affecting the torsional modal response of a Load Commutated Inverter (LCI) driven motor-compressor, and gives practical guidelines for system design optimization. Besides, when the equipment inherent damping properties are not sufficient to achieve demanding vibration performances, an active control could be required: the real implementation of an active damping control system acting on the VSDS is therefore presented, showing its effectiveness on the torsional behavior of a real string by means of experimental results.

Simulations and field test results are herein presented, emphasizing the importance of torsional modal response optimization, considering mechanical aspects and mostly analyzing electrical and control influence introduced using a VSDS. It is worth to highlight that the type of VSDS covered in the paper is the LCI, but the presented system design approach is in principle applicable to any VSDS topology, with specific electrical and control aspects to be considered for each drive.

INTRODUCTION

The reliability of rotating machinery is strongly affected by its torsional behavior since torsional resonances occurring during transient or continuous operations can jeopardize system operability. Vibrations induced by resonant phenomena result in gear noise/vibration and/or coupling wear and in worst cases in shaft line damages in reason of shrink fit slippage, keys failures, gear tooth failures. This is of particular concern when dealing with geared trains since gear meshing can translate torsional vibrations into lateral ones and, more in general, dynamics may easily involve both flexion and torsion.

According to API standards and companies' design practices, to avoid any problem, systems should be engineered in order to avoid intersections between torsional critical speeds and possible excitations within normal operating ranges. On the other hand, wide operability ranges and the need of transient operations such as startup, together with different possible excitation sources, make a torsional detuning not always possible.

If resonances cannot be avoided, the reliability of rotary equipment will rest on the system response magnitude, which depends on torsional alternate inputs magnitude and on the whole train properties, i.e. how inputs are processed by the whole system, resulting in train torsional damping.

Corbo et al. [9] provide a comprehensive list of all the possible internal and external contributions to torsional damping that a system may exhibit: hysteretic damping contribution is usually minor for the frequencies involved in typical moto-compressor geared trains. Instead, even in the absence of combined flexural lateral-torsional dynamics, a gear can induce a kinematic interaction between flexural and torsional dynamics, thus making the support journal bearings become torsional damping actors. Finally, the torsional behavior of the train can also be affected by train resistant load.

The above-mentioned contributions are all passive in nature, and their individual impact on the overall system damping is not straightforward to identify. Experience indicates that a practical way of describing mathematically the mechanical damping of rotating equipment is through the equivalent modal damping of the most significant torsional modes, that can be determined experimentally from a logarithmic decay calculation following a transient event as a unit trip.

In case of a VSDS-driven application, the overall modal damping can be dramatically affected by the dynamics of the Variable Frequency Drive (VFD) controls and electrical circuits.

The impact of both mechanical and electrical contributions on the train torsional modal response of a LCI-driven geared compressor is herein investigated and thoroughly evaluated. Finally, it is demonstrated how the implementation of an active damping control system can be used to govern the overall modal damping to meet demanding torsional vibration performances, as well as induced lateral vibrations on the gearbox, enabling the use of the entire machine operating speed range without speed bands restrictions.

BACKGROUND AND THEORY

The fundamental concepts on torsional dynamics of rotating equipment are hereafter presented, thus providing a suitable background to understand the key aspects governing the torsional modal response in a LCI driven motor-compressor shaft line.

Torsional Dynamic Equations

The generic 2nd order system of differential equations which describe the shaft torsional dynamic behavior of an *N*-dimensional multi-degree-of-freedom system is represented by Equation (1):

$$[J]\underline{\ddot{\vartheta}} + [D]\underline{\dot{\vartheta}} + [K]\underline{\vartheta} = \underline{T} \qquad (1)$$

where $\underline{\vartheta}$ is the angular degrees of freedom vector, $[J]$ is the polar mass moments inertia matrix, $[D]$ is the torsional damping matrix, $[K]$ is the torsional stiffness matrix and $\underline{T}$ is the vector of applied torques. In order to quantify the effect of the torsional damping on the train response, it is useful to introduce the modal approach, representing Equation (1) in terms of modal references through the following coordinate transformation:

$$\underline{\vartheta} = [\Phi]\underline{q} \qquad (2)$$

where $\underline{q}$ is the vector of the modal coordinates and $[\Phi] = [\underline{\varphi}^{(1)}, \dots, \underline{\varphi}^{(i)}, \dots, \underline{\varphi}^{(N)}]$ is the mode-shapes matrix, collecting column-wise the N complex eigenvectors $\underline{\varphi}^{(i)}$ of the system in Equation (1). Combining the above equations and pre-multiplying by the transpose of $[\Phi]$ results in the complex and diagonal system:

$$[\Phi]^T[J][\Phi]\ddot{\underline{q}} + [\Phi]^T[D][\Phi]\dot{\underline{q}} + [\Phi]^T[K][\Phi]\underline{q} = [\Phi]^T\underline{T} \qquad (3)$$

The damping matrix $[D]$ is hard to determine and the definition of complex eigenvectors is not always possible. One can therefore consider the eigenvectors $[\Phi]$ of the undamped system ($[J]\ddot{\underline{\vartheta}} + [K]\underline{\vartheta} = \underline{0}$). Equation (3) becomes:

$$[J_{mod}]\ddot{\underline{q}} + [D_{mod}]\dot{\underline{q}} + [K_{mod}]\underline{q} = \underline{T}_{mod} \qquad (4)$$

where the modal matrices $[J_{mod}]$ and $[K_{mod}]$ are real and diagonal, and $\underline{T}_{mod}$ is the real vector of modal torques. The modal damping matrix $[D_{mod}]$ is assumed diagonal, based on the assumption of weakly-damped system. In analogy with the one-degree of freedom mechanical system one can define a modal damping coefficient ξ_i such that the diagonal (and only non-zero) i^{th} term of this matrix is:

$$D_{mod,i} = 2 \cdot J_{mod,i} \cdot \omega_i \cdot \xi_i \qquad (5)$$

where $J_{mod,i} = \underline{\varphi}^{(i)^T}[J]\underline{\varphi}^{(i)}$ is the modal inertia value, $\omega_i = (K_{mod,i}/J_{mod,i})^{1/2}$ is the torsional natural frequency, and ξ_i is the modal damping ratio, all related to the ith torsional mode ϕ_i. Starting from amplification factor (AF) values coming from field testing activities, the damping ratio can be obtained as:

$$\xi_i = \frac{1}{2 \cdot AF_i} \qquad (6)$$

While the inertia and stiffness coefficients for a shaft line can be easily obtained from equipment manufacturer drawings and data, the torsional excitations composing the $\underline{T}$ vector, as well as the modal amplification factor values for the modes of concern are not as straightforward to quantify. In the next Sections, relevant methods for analysis and field testing activities are provided.

LCI Drive Torsional Excitations

The shaft line under analysis is composed by a synchronous motor (SM) fed by a LCI drive, a speed increaser gearbox and two centrifugal compressors (CC1 and CC2), as shown in Figure 1.
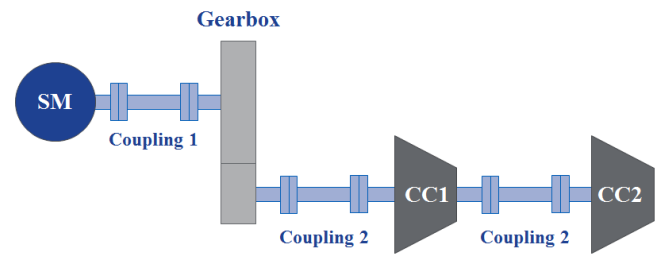

Figure 1 Shaft Line Composition

For a Load Commutated Inverter drive, the resulting torsional excitations occur at specific frequencies, depending on the converter topology. The LCI drive presently analyzed is composed by two electrically independent (magnetically coupled) 6-pulse branches system feeding a 6-windings synchronous motor, as shown in Figure 2.
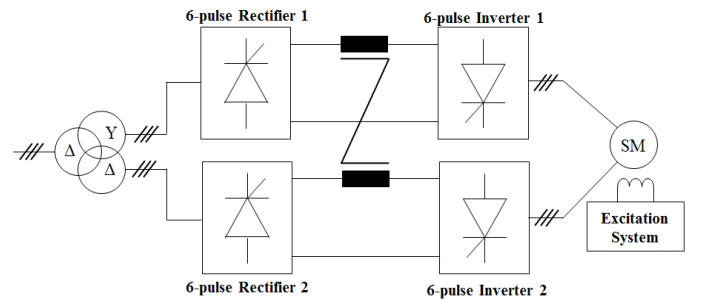

Figure 2 LCI Drive Schematization

The most relevant resulting motor air gap torque excitations can be defined with the following equations:

$$\begin{aligned} y &= 12 \cdot f_M \\ y &= |6 \cdot f_N - 6 \cdot f_M| \\ y &= |6 \cdot f_N - 18 \cdot f_M| \\ y &= |12 \cdot f_N - 12 \cdot f_M| \end{aligned} \qquad (7)$$

where f_N is the network frequency and f_M is the motor frequency. Figure 3 shows the resulting Campbell Diagram, where intersections between the 1st Torsional Natural

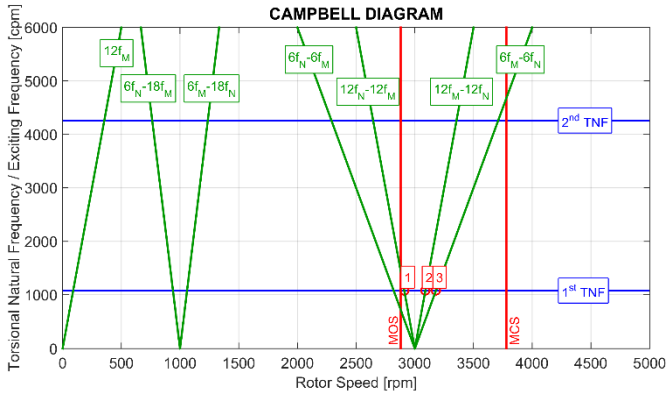Frequency (TNF) and LCI drive inter-harmonics excitations are identified with red labels numbered from 1 to 3.

Figure 3 Campbell Diagram with LCI Drive Excitations

The only TNF of concern for this application is in fact the first one as determined after a careful analysis of the resulting torsional mode shapes. Figure 4 and Figure 5 depict the normalized first and second torsional mode shapes for the system.
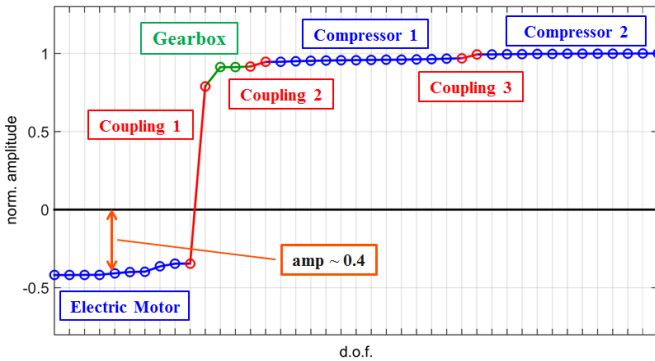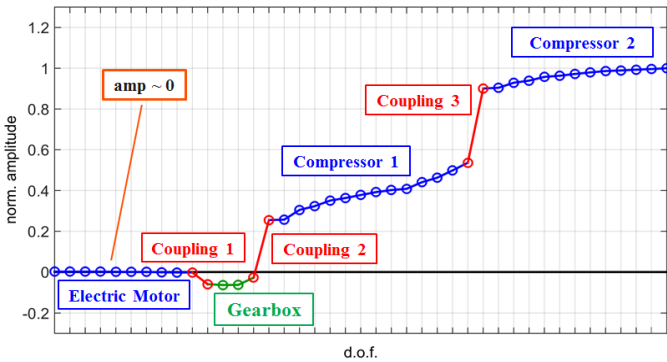

Figure 4 First Torsional Mode Shape (~100 rad/s)

Figure 5 Second Torsional Mode Shape (~450 rad/s)

From Equations (3) and (4) it results that the motor air gap torques, when crossing the first and second torsional modes, can be written as per Equation (8).

$$T_{mod\ 1}^{EM} = \varphi_{EM}^{(1)} \cdot T_{EM}(f = 1^{st}\ TNF)$$
$$T_{mod\ 2}^{EM} = \varphi_{EM}^{(2)} \cdot T_{EM}(f = 2^{nd}\ TNF) \tag{8}$$

where:

$\varphi_{EM}^{(1)}$ and $\varphi_{EM}^{(2)}$ are the amplitudes of the first and second torsional modes in correspondence of the motor windings sections respectively.

$T_{EM}(f)$ is the actual motor pulsating air gap torque at a given frequency.

$T_{mod\ 1}^{EM}$ and $T_{mod\ 2}^{EM}$ are the projections of the actual motor torque excitation on the first and second torsional modes respectively.

From Figure 4 and Figure 5 it results that $\varphi_{EM}^{(1)}$ and $\varphi_{EM}^{(2)}$ amplitudes, normalized with respect to their maximum value, are about 0.4 and 0 (almost a nodal point) respectively for the first and second mode. Therefore, any pulsating torsional excitation arising from the motor at the frequency equaling the 1st TNF is scaled by a scaling factor of about 40%, while if the frequency of excitation is corresponding to the 2nd TNF, such scaling factor is close to zero (the same is applicable to higher order modes). Thus, any excitation at that frequency produces negligible effect on the torsional response of the mechanical system.

Closed-Loop Torsional Interaction

The amplitude of the motor excitations described in the previous section is a function of electrical and control parameters of the whole VSDS, composed by the input transformer, the VFD and the electric synchronous motor. The analytical computation of such amplitudes is not straightforward and it is normally obtained from complex simulations including detailed models of all the items composing the VSDS.

When the LCI drive is coupled with the moto-compressor system, torsional closed-loop interactions occur. This means that whenever the spectrum of the torque forcing function $T(f)$, originating from the electric motor, contains enough energy in bands comprising at least one TNF of the moto-compressor train, the train itself will undergo torsional oscillations. These appear also as speed oscillations $\Omega(f)$ at the motor shaft.

Such speed oscillations $\Omega(f)$ in turn produce voltage and current oscillations at motor terminals because of the electromagnetic interaction between rotor and stator parts in the motor itself.

Additionally, voltage oscillations on the AC side of the inverter results in voltage oscillations on the DC side of the inverter $v_{DC,inv}(f)$, because of the inherent working principle of the converter. Ultimately, the DC link current of the LCI VSDS, $I_{DC}(f)$, is affected by the inverter DC voltage

oscillations as shown in Figure 6. From this schematic view, Equation (9) (Bose B. K. [8]) is derived:

$$i_{DC} = \frac{1}{L} \cdot \int \left(v_{DC,rect} - v_{DC,inv} \right) dt \qquad (9)$$

where L is the DC link inductance (DC link resistance is negligible for large machines), $v_{DC,rect}$ is the rectifier side DC voltage and $v_{DC,inv}$ is the inverter side DC voltage.
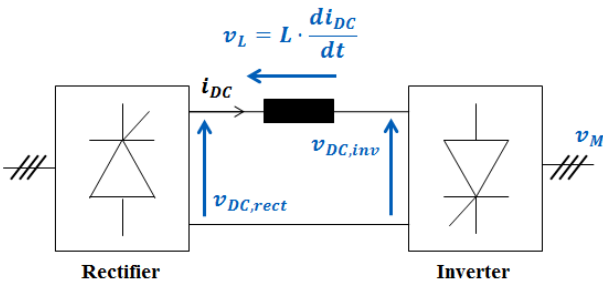

Figure 6 Schematic view of LCI Drive DC link

The main VFD control loop affecting the torsional interactions phenomena is the DC link current regulator, whose purpose is to keep the DC link current at a given reference $i_{DC,ref}$, by acting on the firing angles of the rectifier thyristors, to generate the desired motor average torque. In a simplified way, this can be represented by a Proportional-Integral (PI) Regulator that in turn defines the required firing angle for the rectifiers' thyristors, as shown in Figure 7.
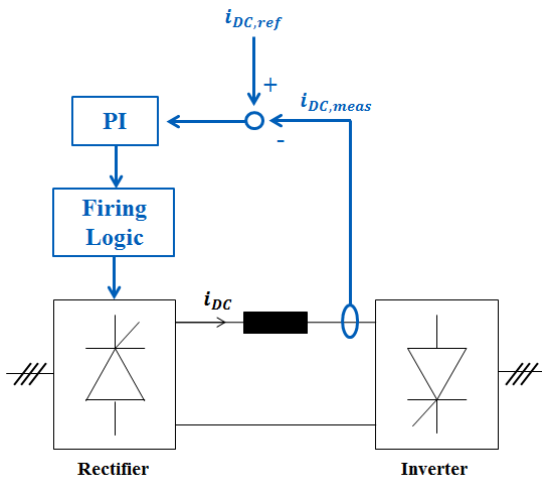

Figure 7 Schematic view of DC link Current Regulator

Since the measured DC link current $i_{DC,meas}$ is affected by the inverter DC voltage oscillations, the PI regulator perceives this as a disturbance on the DC link current and therefore it will try to react to that disturbance, because its purpose is to keep the DC link current constant. Figure 8 depicts a schematic of the resulting DC link current transfer functions.
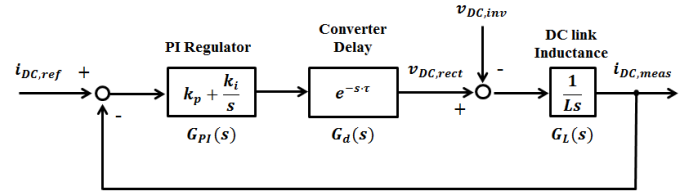

Figure 8 Schematic view of DC link Transfer Functions

The resulting *open loop* transfer function $G(s)$ is written as:

$$G(s) = G_{PI}(s) \cdot G_d(S) \cdot G_L(s)$$
$$G_{PI}(s) = k_p + \frac{k_i}{s}$$
$$G_d(s) = e^{-s \cdot \tau} \qquad (10)$$
$$G_L(s) = \frac{1}{L \cdot s}$$

where τ is the delay introduced by the converter, which is dominated by the nature of each single thyristor that can commutate once each half fundamental period, at most. Since six thyristors are present in each 6-pulses bridge and they commutate in sequence, with a transition occurring every 1/6th of the fundamental period, τ is approximated as half of the period of the sixth harmonic (Bose B. K. [8]):

$$\tau = \frac{1}{2} \cdot \frac{1}{6 \cdot f_{line}} \qquad (11)$$

where f_{line} is the Rectifier input voltage frequency. Introducing the factory parameters for the LCI drive analyzed in this paper, the Bode plot of the DC link transfer function $G(s)$ appears as shown in Figure 9.
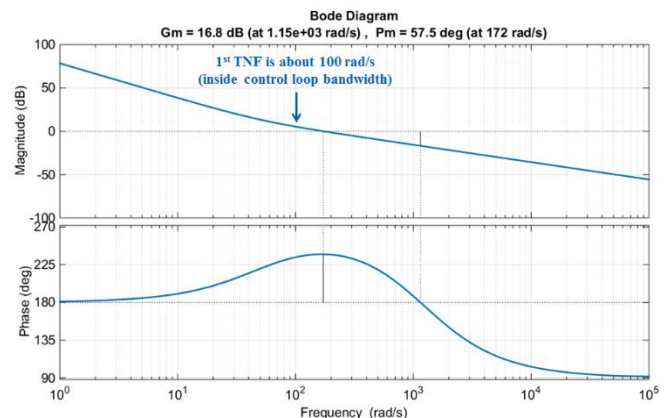

Figure 9 DC Link Transfer Function Bode Plot derived from Factory Parameters

From this Bode plot it results sufficiently positive phase margin (57.5°) and gain margin (16.8 dB) to guarantee stable behavior of the control system. The resulting Bandwidth is 172 rad/s, i.e. about 27 Hz. This means that any disturbance below

this frequency (including the 1st TNF of the moto-compressor train under analysis) will affect the overall behavior of the DC link current control loop.

The capability to reject a disturbance for a control loop as the one shown in Figure 8 can be estimated by analyzing the resulting transfer function (Disturbance Sensitivity Transfer Function) between the disturbance ($v_{DC,inv}$) and the output, which is the resulting DC link current $i_{DC,meas}$, as defined in Equation (12) (Ogata K. [5]).

$$S(s) = \frac{G_L(s)}{1 + G(s)} \qquad (12)$$

The resulting Bode plot for the current application considering the factory parameters is shown in Figure 10.

At the frequency of the 1st TNF (~100 rad/s), the magnitude in dB of such transfer function is positive, meaning that this disturbance is amplified.
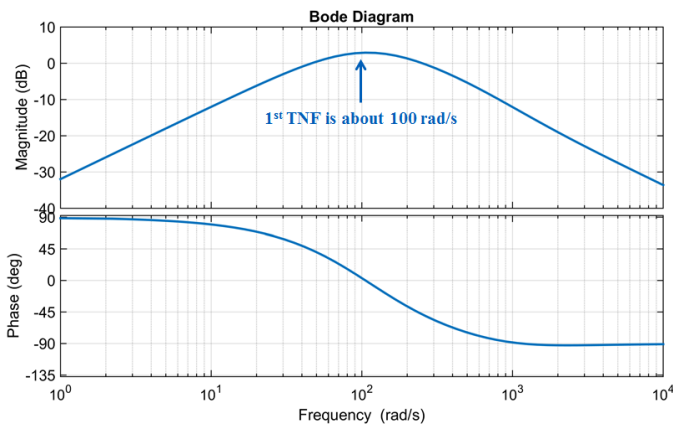

Figure 10 DC Link Sensitivity Function – Factory Parameters

In the *LCI Control Parameters Tuning* Section, a method to improve the capability of the DC link current control loop to reject a disturbance is presented.

Gearbox Bearings Effects on Torsional Damping

The gear journal bearings can affect the train torsional dynamics because of variations in load, speed and oil temperature. These parameters are mainly supposed to affect the gear lateral dynamics. On the other hand, torsional vibrations can also be affected: the bearings can be important actors in torsional damping when lateral displacement accompanying the torsional vibration due to the arm between the meshing force vector and the journal bearing reaction force vector. Indeed, based on a viscous point of view the contribution of the bearing would be negligible, but when a kinetic coupling is considered at the mesh, the lateral vibration induced by the radial load at the gear mesh cause the oil to create a squeeze film effect that can have consequences on

torsional behavior. Of course, if one focuses on a torsional resonance condition excited by the LCI drive inter-harmonics, the speed becomes a constant and the gear bearing properties will depend on load and oil temperature. In this paper the effect of both load and temperature will be investigated.

SYSTEM DESIGN AND OPTIMIZATION

The main system design aspects and optimization criteria in terms of torsional dynamics of the train under analysis are hereafter presented.

Torsional Analysis Simulations Results

The system is characterized with an equivalent lumped parameters torsional model represented in Figure 11.
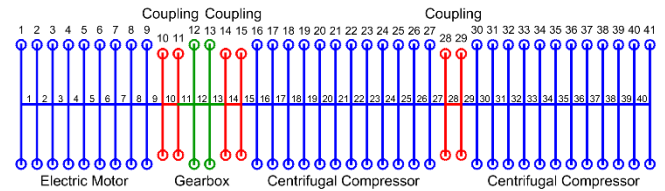

Figure 11 Lumped Parameters Equivalent Single-Line Torsional Model. Gear ratio 2.7.

During the engineering phase a detailed torsional analysis was carried out. The resulting Campbell Diagram is shown in Figure 3. The most relevant intersections between the train torsional natural frequencies and the LCI drive excitations are summarized in Table 1, as described in the LCI Drive Torsional Excitations Section. The related speeds are defined in [pu] of the motor rated speed (1 [pu] = rated speed).

#	Excitation	Speed [pu]
1	$12 \cdot f_N - 12 \cdot f_M$	0.81
2	$12 \cdot f_M - 12 \cdot f_N$	0.86
3	$6 \cdot f_M - 6 \cdot f_N$	0.88

Table 1 Campbell Diagram Intersections with 1st TNF. f_M is the motor frequency, f_N is the network frequency

A forced response analysis was carried out to perform an infinite fatigue life assessment of the overall shaft line in those conditions. The forced torsional response was calculated through a detailed simulation model, with the entire VSDS including the input step-down transformer, the LCI converter and the synchronous motor along with its excitation system (Figure 12), coupled with the detailed train torsional model (as described in the *Torsional Dynamic Equations* Section).

With this simulation model, the resulting motor air gap torque excitations were computed for each speed of intersection in the Campbell Diagram considering the motor at rated load, and applied on the motor windings sections of the torsional model and the centrifugal compressor loads were

modeled through their torque vs. speed curves. The maximum expected motor average torque for the speeds of analysis was used. The torsional damping effects were included in terms of modal amplification factors according to internal design practice values.
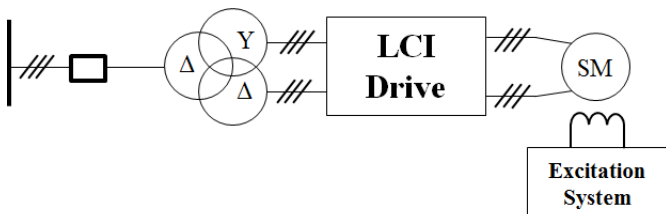

Figure 12 LCI Drive Simulation Model Scheme

The resulting torsional response was calculated for all the shaft line components and verified with their respective infinite fatigue life thresholds. The weakest element of this train is the motor side coupling and for that element the resulting alternate torque at the frequency of the 1st TNF in the worst analyzed scenario is about 31% of the motor rated torque. The corresponding waterfall plot is shown in Figure 13 as [pu] of the motor rated torque (1 [pu] = rated torque).
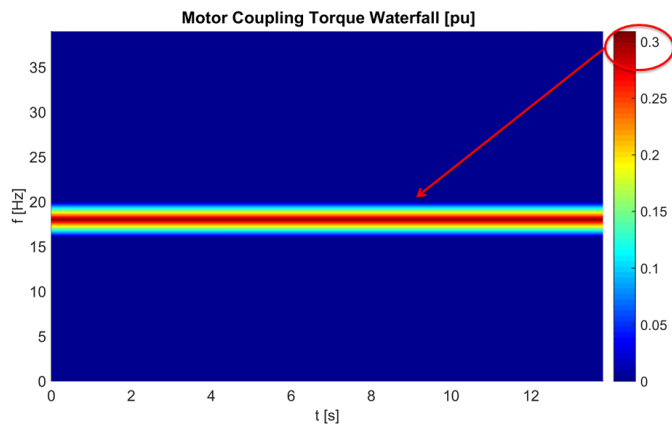

Figure 13 Motor Coupling Torque Waterfall Plot - Forced Response Worst Case Prediction at ~100 rad/s

The infinite fatigue life assessment was widely verified, as shown in the motor side coupling Goodman Diagram in Figure 14. Even if the infinite fatigue life assessment was satisfactory, the project requirement from Customer for this specific application was slightly above the calculated motor alternating in the worst operating scenario (about 0.32 [pu]). In addition, the gearbox lateral vibrations with the system in the worst torsional resonance condition were computed, obtaining the expected sub-synchronous vibration amplitudes, with a maximum value of about 10µm peak-to-peak. The maximum allowable limit in terms of any non-synchronous vibration was 7µm peak-to-peak. Therefore, under torsional resonance condition, the predicted values of both torsional vibration amplitude on motor coupling and gearbox lateral vibrations

were very close to the string test acceptance criteria, therefore the risk to fail the test was serious.
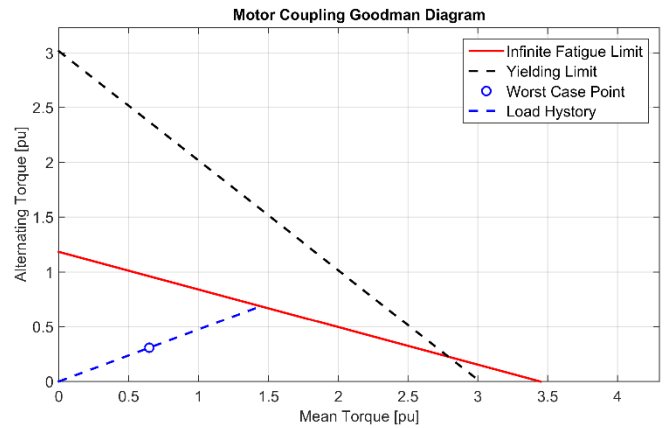

Figure 14 Motor Coupling Goodman Diagram

LCI Control Parameters Tuning

As described in the *Closed-Loop Torsional Interaction* Section, the capability to reject a disturbance for a control loop as the one shown in Figure 8 can be estimated by analyzing the Disturbance Sensitivity Transfer Function (Equation (12)).

Among the simplest ways to potentially increase the capability to reject a disturbance within the DC link control loop bandwidth is the increasing of the bandwidth itself. This can be done by increasing the proportional gain k_p of the PI regulator, which also improves the Phase margin up to a certain frequency that in this case is about 230 rad/s. Above this threshold, the Phase margin starts decreasing with an increasing bandwidth, thus reducing the stability margin of the control system. For this application, the best compromise between stability margin and capability to reject a disturbance is achieved by obtaining a bandwidth of 232 rad/s, i.e. about 37 Hz.
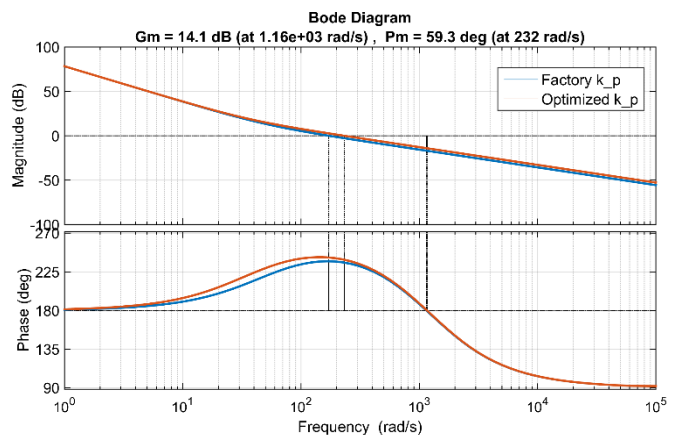

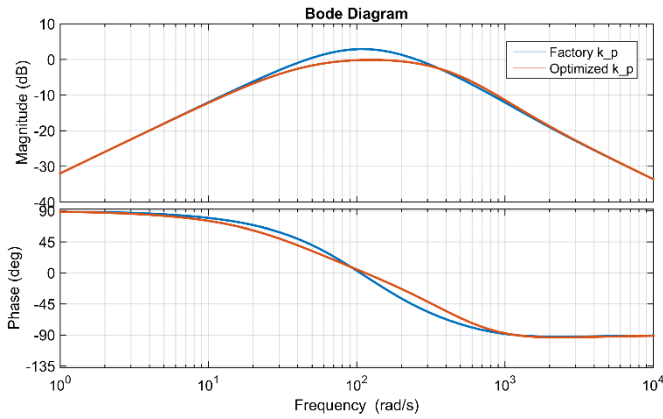**Figure 15 DC Link Transfer Function Bode Plot – Optimized Parameters**

Figure 16 DC Link Disturbance Sensitivity Transfer Function – Optimized Parameters

Figure 15 and Figure 16 show the Bode plots of the optimized control system (red line) vs. factory control parameters (blue line) in terms of DC link open loop transfer function and sensitivity transfer function. From the sensitivity transfer function across the frequency range where the 1st TNF lies for this application it results that the magnitude in dB of this function moved from about 2.9dB to about -0.14dB. Considering the dB magnitude definition:

$$|S(j\omega)|_{dB} = 20 \cdot \log_{10} M_{ph} \qquad (13)$$

the resulting physical gain M_{ph} between input (disturbance) and output (DC link current) of the sensitivity transfer function at the frequency of the 1st TNF for the factory and optimized parameters results:

$$M_{ph,factory} = 10^{\frac{2.9}{20}} \approx 1.39$$
$$M_{ph,optim} = 10^{-\frac{0.14}{20}} \approx 0.98 \qquad (14)$$

Finally, with the factory control settings the disturbance at the frequency of the first TNF is amplified by about 39% while with the optimized tuning such disturbance is slightly attenuated by about 2%. In the end, moving from the factory parameters to the optimized ones, the disturbance at the frequency of the 1st TNF is reduced by about 29%. This is reflected by the resulting motor torsional excitation (proportional to the current, considering small perturbation across a linearized system) in resonance condition with the 1st TNF of the train, as demonstrated by the field experiences hereafter described.

Active Damping Control System

The LCI Control Parameters tuning for this application is expected to be not sufficient to meet the project requirements in terms of alternating torque on motor coupling and gearbox sub-synchronous lateral vibrations.

It was agreed with Customer to implement and test an Active Damping Control System for the train String Test (Sihler C. [7]) as mitigation action. The system architecture is shown in Figure 17.
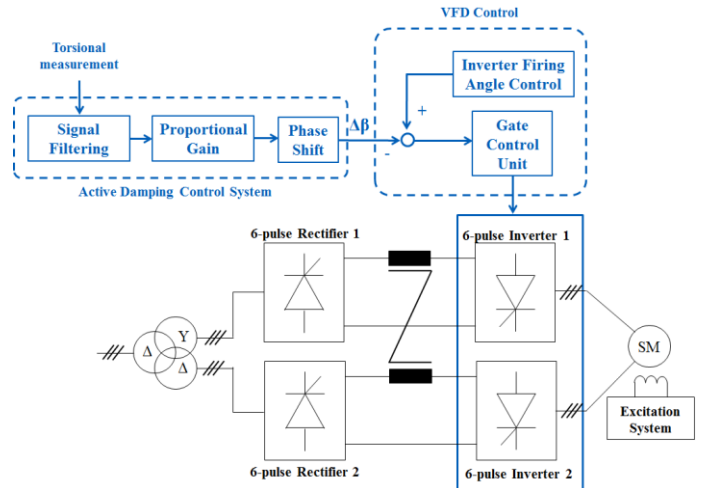

Figure 17 Active Damping Control System Architecture

Basically, the instantaneous alternating torque is measured through a torque-meter system (refer to *Torsional Measurement System* Section for details), and sent to the Active Damping Control System. Proper signal filtering across the train 1st TNF is carried out and a suitable proportional gain is applied to properly define how fast the system reacts to damp a torsional vibration. Finally, the phase shift value needs to be properly configured to have an output signal opposite in phase with respect to the input signal. The output signal of the Active Damping Control System is a correction *ΔB* to be applied on the firing angle of the inverters of the LCI drive. This modulation has the effect of producing a frequency component of the motor air-gap torque opposite in phase with respect to the mechanical torsional vibration, thus obtaining a damping effect.

Mathematically this is equivalent to adding a forcing function at the right-hand side of Equation (4). that, when transferred at the left-hand side of the same Equation, produces a damping term of greater magnitude. This is the common principle of several active damping solutions and it is applied here by using the electrical drive as controlled actuator on the train. This is technologically possible nowadays because the dynamics of the power electronic converters is significantly faster than the relevant torsional dynamics in the vast majority of Multi-Megawatt trains. The principle would not have been technologically applicable in the past so effectively, when purely mechanical actuators only would have been selected to materialize the same principle. This simply because their control dynamics would have not been able to be significantly faster than the torsional ones, like the power-electronic converters can easily achieve.

TEST BED SET-UP

A dedicated test campaign was carried out with the intent to evaluate the effects of the key factors affecting the torsional modal response of the LCI driven moto-compressor train under analysis and to test the Active Damping Control System. A description about the measurement system for both mechanical and electrical quantities of concern follows.

Torsional Measurement System

The test bench equipment for torque measurement consists in a torque-meter and string gauges used to validate the torque meter accuracy.
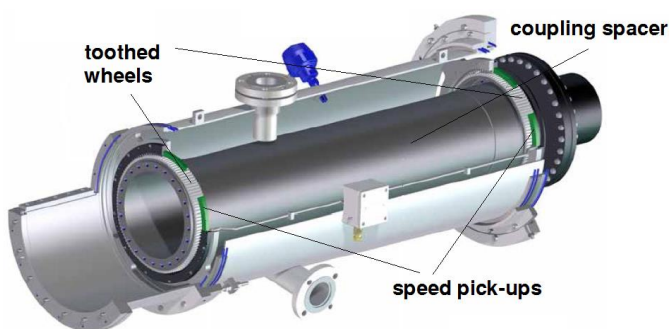

Figure 18 - Torque-Meter Cross-Section

Figure 18 shows a schematic isometric view of the torque-meter that allows estimating the mean and alternate torque experimented by the motor-side coupling (T_{TM}) by measuring a phase shift $\Delta\theta$ between two track-teeth sections placed at the spacer ends. The phase shift can be read as a torque if one considers the spacer torsional stiffness k_t, i.e. from:

$$T_{TM} = k_t \cdot \Delta\theta \qquad (15)$$

Figure 19 depicts the (two) strain gauge rosettes (installed at 180°) on the coupling spacer, gearbox side, connected in a full bridge configuration.
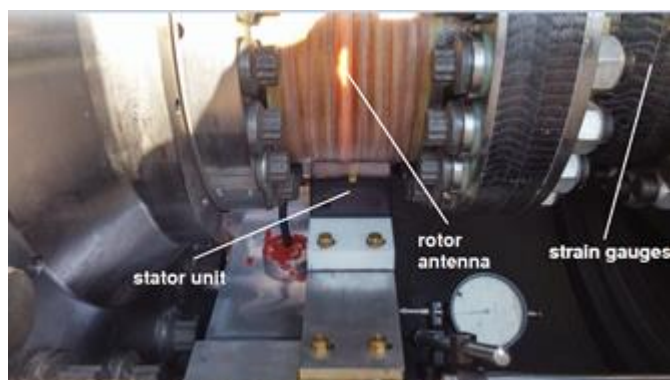

Figure 19 - Strain Gauges Installation on Motor Side Coupling

The strain gauges are connected to a rotor antenna transmitting the signal to a stator unit. The unbalance of the Wheatstone bridge circuit made of resistive foils due to deformation is transmuted into a voltage corresponding to a certain torque magnitude once material elastic properties are considered. One can see the transmitting rotor antenna device in the middle (in red) in Figure 19. The black block on the bottom is the receiving stator unit. In black, on the right, the Wheatstone bridge installation (strain gauges).
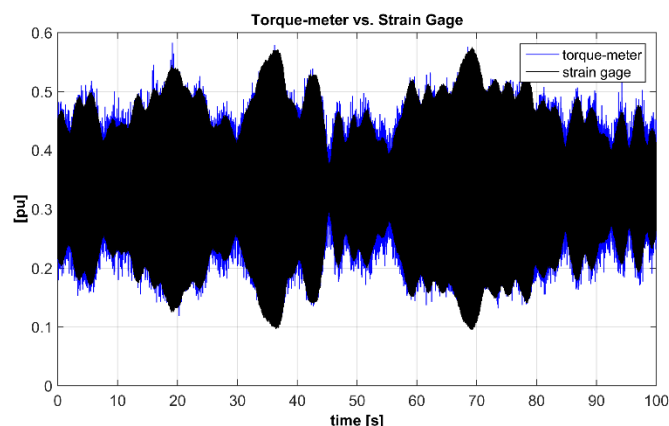

Figure 20 Comparison of Torque-meter vs. Strain Gauge Torque Outputs

The measurements coming from the strain gauges resulted to be well in agreement with the torque-meter output in terms of envelope, as shown in Figure 20, obtained from a resonance condition analysis. All the test results shown in the following are based on torque-meter output signals, being such device permanently installed for torsional monitoring of the unit as requested by the Customer.

Electrical Measurement System

The estimation of the electric motor air gap torque is essential to determine the actual pulsating torque exciting the shaft line. Among others, the following instrumentation is available for such purpose (ref. Figure 21):
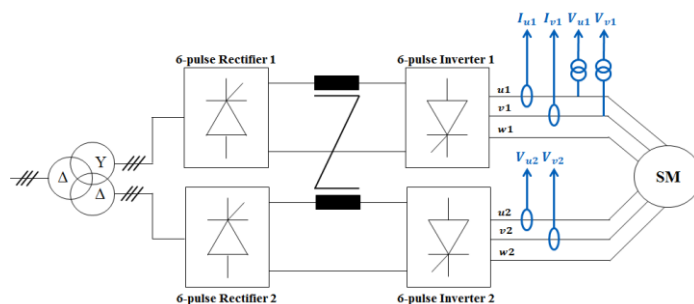

Figure 21 Electrical Measurements for estimation of motor air gap torque

- 2 current transformers (CTs) to measure Inverter 1 output currents for phase $u1$ and $v1$ ($I_{u1}(t)$ and $I_{v1}(t)$)
- 2 voltage transformers (VTs) to measure Inverter 1 output voltages for phase u1 and v1 ($V_{u1}(t)$ and $V_{v1}(t)$)
- 2 current transformers (CTs) to measure Inverter 2 output currents for phase u2 and v2 ($I_{u2}(t)$ and $I_{v2}(t)$)

By means of these measurements, the overall 6-phase electrical quantities in terms of currents and voltages can be estimated assuming identity for the two motor three-phase windings, which is a reasonable hypothesis for large electrical machines in the Multi-Megawatt range where high accuracy in the analyses is not needed. Assuming a balanced and symmetric three phase system, current and voltage amplitudes for phase w_1 are obtained as $I_{w1} = -I_{u1} - I_{v1}$ and $V_{w1} = -V_{u1} - V_{v1}$. Similarly, for the current of phase w_2 related to the second branch $I_{w2} = -I_{u2} - I_{v2}$.

Since no voltage measurements are taken for the Inverter 2 outputs, those are calculated by shifting of 30 electrical degrees the Inverter 1 output voltages, being the two branches of the LCI basically identical but with line side voltages 30 electrical degrees shifted because the two secondary windings of the input step-down transformer have respectively Y and Δ connections. This result in a time delay applied to the Inverter 1 output voltages obtained as per Equation (16).

$$t_{delay} = \frac{2\pi}{\omega_{line}} \cdot \frac{30°}{360°} \quad (16)$$

where ω_{line} is the line side pulsation. Inverter 2 output voltages are therefore calculated by delaying Inverter 1 voltages by the above time delay. With both the Inverters output electrical quantities, the resulting instantaneous electrical power entering the motor is calculated as:

$$p(t) = V_{u1}(t) \cdot I_{u1}(t) + V_{v1}(t) \cdot I_{v1}(t) + V_{w1}(t) \cdot I_{w1}(t) + V_{u2}(t) \cdot I_{u2}(t) + V_{v2}(t) \cdot I_{v2}(t) + V_{w2}(t) \cdot I_{w2}(t) \quad (17)$$

When torsional oscillations have frequencies not greater than 1/3 of the electrical fundamental frequency of the motor, than one can fairly assume that the average power over an electrical fundamental period, as computed by Equation (17), is affected by such oscillations and it undergoes a relative variation much greater than the speed, which can be fairly assumed constant and equal to its average value ω_{av}, available as measurement. Therefore, one can approximately estimate the instantaneous machine airgap torque - inclusive of torsional oscillations - via Equation (18).

$$T_{EM}(t) = \frac{P(t) \cdot \eta}{\omega_{av}} \quad (18)$$

where η is the electric motor efficiency.

FIELD EXPERIENCE AND ANALYSIS

Specific analyses on field test data have been carried out, quantifying the effects of the key factors affecting the torsional excitation mechanism and the relevant torsional modal damping contribution, as well as the effect of the Active Damping Control System.

Mechanical Amplification Factor Estimation

As first step of the analysis, the damping of first torsional mode due to the only mechanical effects was estimated, starting from a torsional measurement on the motor side coupling following a trip event (VFD breaker opening). Figure 22 depicts the resulting torque vs. time is and its waterfall plot is shown in Figure 23.
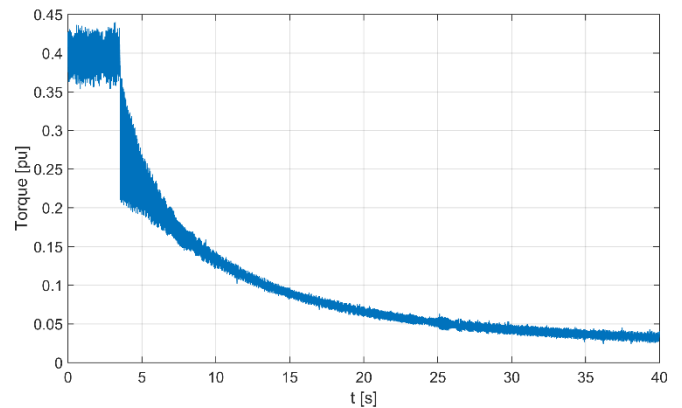

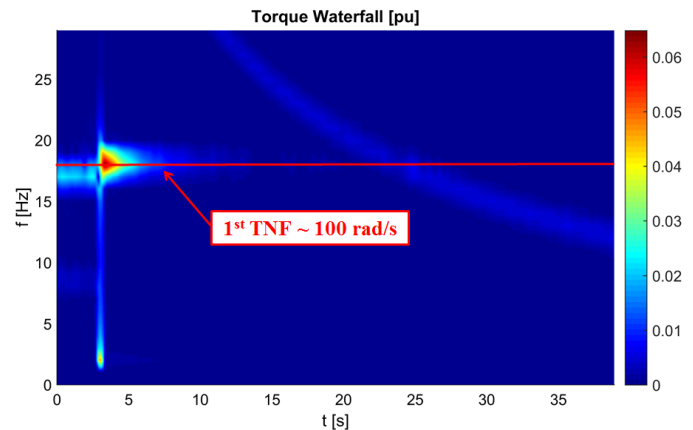**Figure 22 Motor Coupling Torque after a Trip Event**

Figure 23 Motor Coupling Torque after a Trip Event – Waterfall Plot

In order to evaluate the decay of the torsional oscillation related to the first torsional mode, the amplitude of the

previous waterfall plot at the frequency of the 1st TNF was extrapolated (Figure 24).
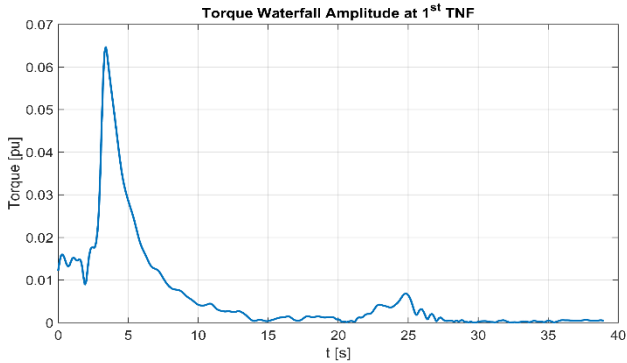

Figure 24 Motor Coupling Torque after a Trip Event – Waterfall Plot Amplitude component at f = 1st TNF vs. time

Figure 22 basically represents the decay amplitude during a free torsional oscillation of the system. The natural base logarithmic is then applied to this signal and the points across the first few seconds after the trip event linearly interpolated, obtaining the red slope shown in Figure 25.
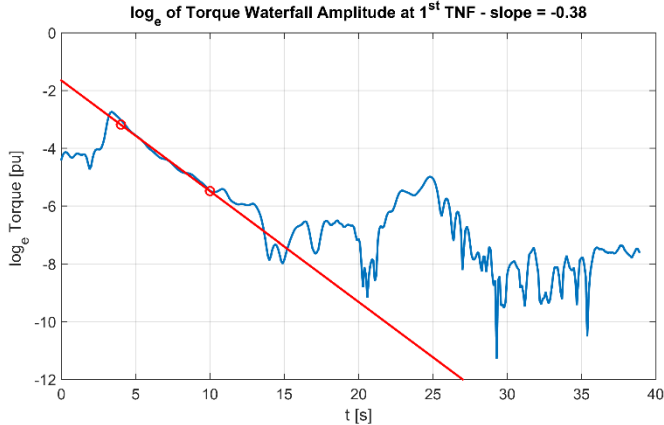

Figure 25 Motor Coupling Torque after a Trip Event – Waterfall Plot Amplitude $\log_e$ at f = 1st TNF

The slope of Figure 25 basically represents the exponential decay of a free torsional oscillation response, as shown in Figure 26. Given the estimated slope $\alpha = -0.38$, the damping ratio ξ and then the related Amplification Factor (AF) are obtained from:

$$\alpha = -\xi \cdot \omega_n \rightarrow \xi = \frac{-\alpha}{\omega_n}$$

$$AF = \frac{1}{2 \cdot \xi} \tag{19}$$

The resulting AF for the first torsional mode is about 150, i.e. very little damping ratio ($\xi \sim 0.3\%$). Note that the unit trip

occurred without venting the compressors. The same test was done with a different load before trip, basically obtaining the same AF.
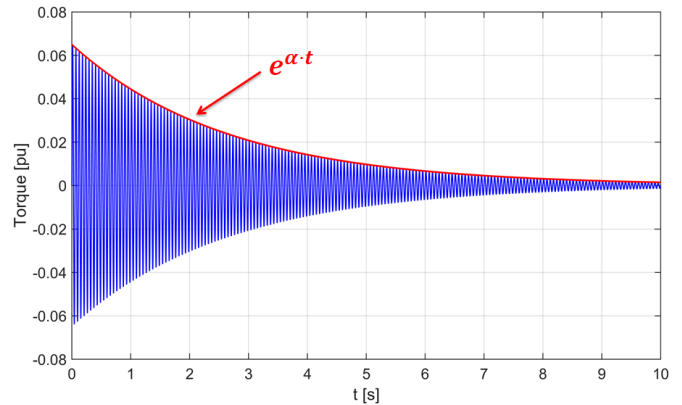

Figure 26 Free Torsional Oscillation response and Exponential Envelope Term

LCI Control Parameters Tuning Validation

As described in the Closed-Loop Torsional Interaction Section, to improve the capability of the DC link current control loop to reject a disturbance inside its bandwidth, the DC current proportional gain k_p can be increased up the maximum value, after which the stability margin starts to decrease. To prove this theoretical analysis, the motor speed was set at the intersection between the $6f_M - 6f_N$ excitation and the 1st TNF of the shaft line (#3 in Table 1). During this resonance condition, the system was kept for few minutes with the LCI drive factory control parameters, and after that the DC link current proportional gain was increased up to the optimum value defined in the analysis described earlier. Figure 27 and Figure 28 show respectively the (waterfall plot) measured motor air gap torque and the measured torque on the motor side coupling across the k_p tuning.
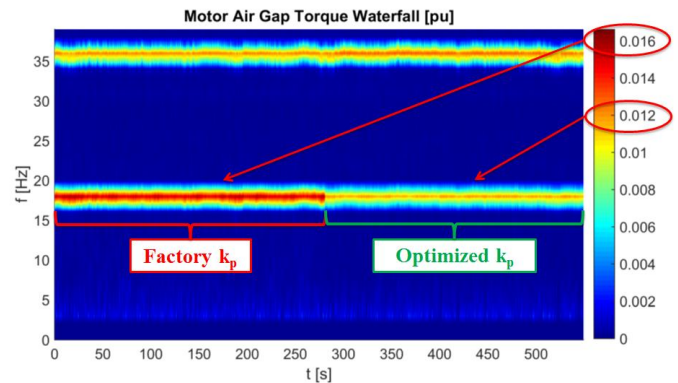

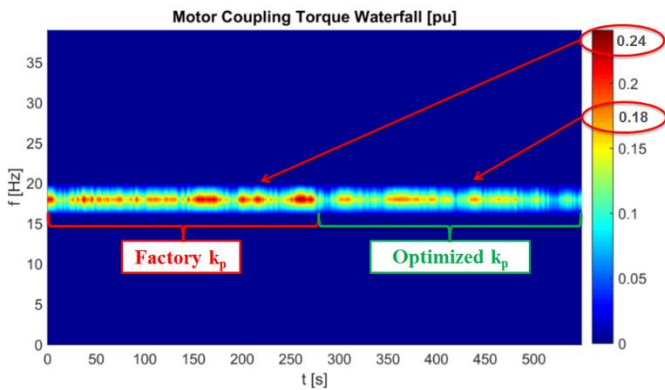**Figure 27 Motor Air Gap Torque Waterfall – k_p Optimization**

Figure 28 Motor Coupling Torque Waterfall – k_p Optimization

The amplitude of the motor air gap torque with the factory proportional gain is about 1.6% of motor rated torque, while with the optimized value it decreases to about 1.2% of motor rated torque. A reduction of about 25% of the motor excitation in resonance condition with the 1st TNF was therefore obtained. It is interesting to point out that the expected theoretical reduction of the 1st TNF disturbance inside the DC link current control loop bandwidth was about 29%, thus the analysis results delivered a very good approximation of the behavior of the real system.

On the other hand, the measured alternating torque response at the motor coupling before and after the control tuning optimization is about 0.24 [pu] and 0.19 [pu], while the simulation results during engineering phase (with factory VFD parameters) lead to an alternating torque on the motor coupling of about 0.31 [pu] with factory control parameters.

Worthy of notice, the ratio between the motor excitation and motor coupling torque before and after the control tuning is basically the same, meaning that the control optimization had the benefit of reducing the torsional excitation with a negligible impact on the overall torsional modal damping.

Overall Modal Amplification Factor Estimation

Once the VFD settings were optimized, the impacts of the compressors load and lube oil bearings inlet temperature on the torsional modal response were also investigated.

The method used to estimate the modal amplification factor under different operating conditions is first described, and the resulting values are presented. Focus was put on all the resonance conditions shown in Table 1. In particular, results for $6f_M - 6f_N$ (#3 of Table 1) and $12f_N - 12f_M$ (#1 of Table 1) inter-harmonics are hereafter presented. Being the $12f_M - 12f_N$ (#2 of Table 1) excitation comparable with the excitation #1, the corresponding results are not shown. In the following, resonance conditions will be referenced as per Table 1.

For intersection #1 in Table 1 two distinct loads were investigated. Once the motor pulsating air gap torque and the resulting motor side coupling torque were measured for one

case, the correspondent amplification factor AF_{test} was found by means of the available torsional model, as described below.

The amplitude of the motor pulsating torque at the frequency of the 1st TNF was first estimated as shown in the *Electrical Measurement System* section. The corresponding waterfall plot is in Figure 29, showing a torsional excitation amplitude of about 0.01 [pu]. The corresponding measured torque on motor coupling is about 0.18 [pu] (Figure 30).
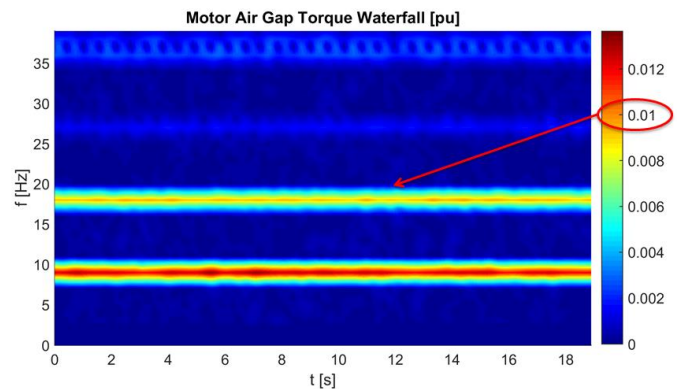

Figure 29 Motor Air Gap Torque Waterfall - 29.8% rated load, Intersection #1
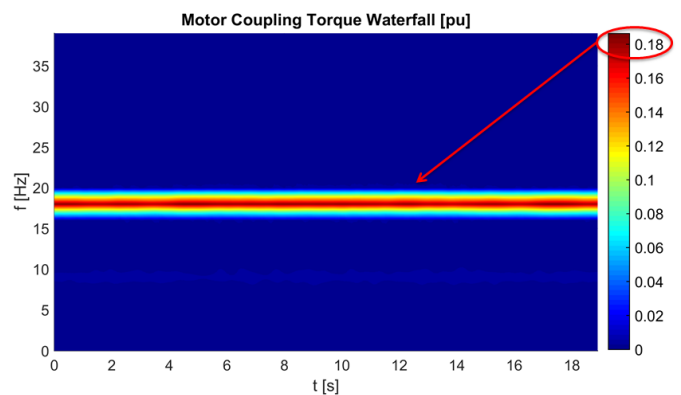

Figure 30 Motor Coupling Torque Waterfall - 29.8% rated load, Intersection #1

This experimentally derived motor input magnitude was then used as amplitude of a harmonic excitation at the frequency of the 1st TNF.
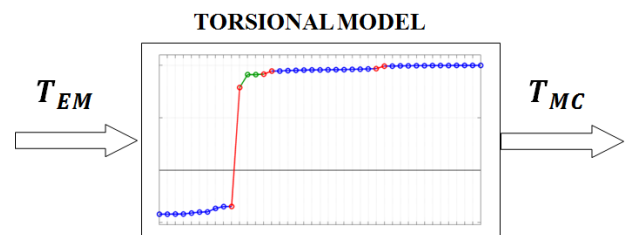

Figure 31 Analytical Motor Coupling Response to the Measured Motor Excitation

The torque response on the motor side coupling was then computed with a modal amplification factor according to internal design practice, as schematically shown in Figure 31, where:

$$T_{EM} = 0.01\,[pu] \cdot sin(\omega_{1TNF}t)$$
$$T_{MC} = T_{MC,cmp}\,[pu] \cdot sin(\omega_{1TNF}t) \qquad (20)$$

Now, based on what described in the *Torsional Dynamic Equations* Section, the torsional response can be evaluated as follows (assuming system linearity):

$$T_{MC,test} = AF_{test} \cdot \phi_{1TNF} \cdot T_{EM,test}$$
$$T_{MC,cmp} = AF_{DP} \cdot \phi_{1TNF} \cdot T_{EM,cmp} \qquad (21)$$

where:

AF_{test} and AF_{DP} are the actual system amplification factor and the one coming from internal design practice respectively.

ϕ_{1TNF} is a coefficient taking into account the modal shape contribution to system response.

$T_{EM,test} = T_{EM,cmp} = T_{EM}$ is the measured alternate motor air gap torque also used for the computation.

$T_{MC,test}$ and $T_{MC,cmp}$ are the actual and computed motor coupling alternate torque respectively.

By dividing Equations (21), one has:

$$AF_{test} = AF_{DP} \cdot \frac{T_{MC,test}}{T_{MC,cmp}} \qquad (22)$$

Once the above is done for this first case, based on the same assumptions, one can then estimate the actual amplification factor for any n^{th} test condition under analysis as follows:

$$AF_{test,n} = AF_{test} \cdot \frac{T_{EM,test}}{T_{MC,test}} \cdot \frac{T_{MC,test,n}}{T_{EM,test,n}} \qquad (23)$$

Table 2 lists the calculated amplification factors for the first torsional mode at the Campbell intersection #1 for different compressors load cases (load is in [pu], with respect to the motor rated power).

12f_N-12f_M Resonance Condition	
Load [pu]	AF
0.30	59.2
0.33	48.7

Table 2 Variation of AF with load at the 12f_N-12f_M resonant condition. Lube oil temp set at 55°C

Additionally, two different loads were investigated at the $6f_M - 6f_N$ resonance condition too. Table 3 shows the resulting amplification factors.

6f_M-6f_N Resonance Condition	
Load [pu]	AF
0.34	65.3
0.43	44.7

Table 3 Variation of AF with load at the 6f_M-6f_N resonant condition. Lube oil temp set at 55°C.

For the sake of clarity, the mentioned conditions refer to the same torsional frequency, excited at different speeds. Both resonant conditions show that the higher the load the lower the amplification factor AF. These results are due both to a load effect on the gearbox journal bearings (considering a coupling between torsional and lateral dynamics) and, more in general, to the resistant load acting in opposition to the shaft line twisting. The results above were performed with a bearings inlet lube oil temperature set at 55°C. The influence of lube oil temperature for both resonant conditions #1 and #3 of Table 1 was investigated too, keeping the load constant. Table 4 summarizes results.

12f_N-12f_M Resonance condition at 0.29 [pu] load		6f_M-6f_N Resonance Condition at 0.46 [pu] load	
Temperature [°C]	AF	Temperature [°C]	AF
45	92.2	45	71.9
55	67.4	55	59.3

Table 4 Variation of AF with lube oil temperature set at 12f_N-12f_M and 6f_M-6f_N resonant conditions

Vibrations Measurements

Gearbox low speed (LS) and high speed (HS) shaft radial direct vibrations – drive end (DE) and non-drive end (NDE) – and coupling torque time trends are analyzed for the $12f_N - 12f_M$ intersection (gear shafts scheme shown on Figure 32).
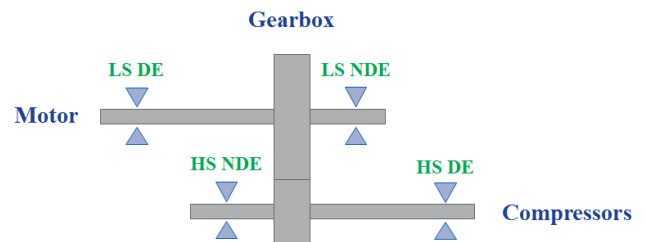

Figure 32 Gearbox Bearings Schematic

In particular, Figure 33, Figure 34 and Figure 35 show the zero-peak trend of above mentioned signals. For the same resonant conditions, the waterfall plots of gearbox shaft DE sides' lateral vibration (horizontal direction) and coupling torques are shown in Figure 37 through Figure 42.

It is to point out that, despite the speed reference was set at the desired constant value, the maximum amplitude of the analyzed quantities appears to be not continuous throughout the considered time range (more than 15 minutes). This can be

addressed to the narrow-like shape of the frequency response function (FRF) around the resonance frequency. Therefore, the system is very sensitive to even very small variations of the actual speed (i.e. very small variations of the electric motor exciting frequency), which lead to large changes on the resulting output amplitudes, as shown in Figure 36.
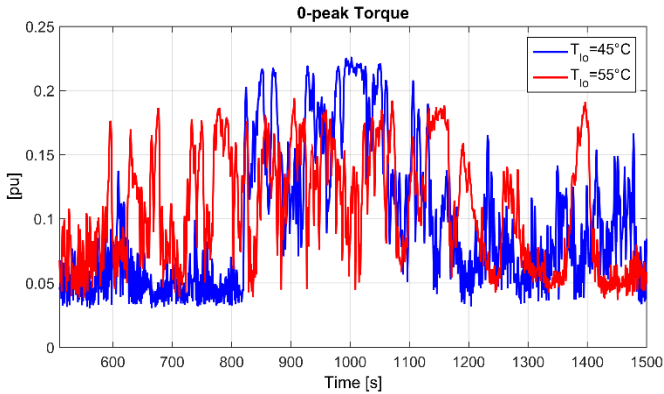

Figure 33 Torque 0-peak trend at the 12f$_N$-12f$_M$ resonant condition. Compressors load 0.29 [pu]
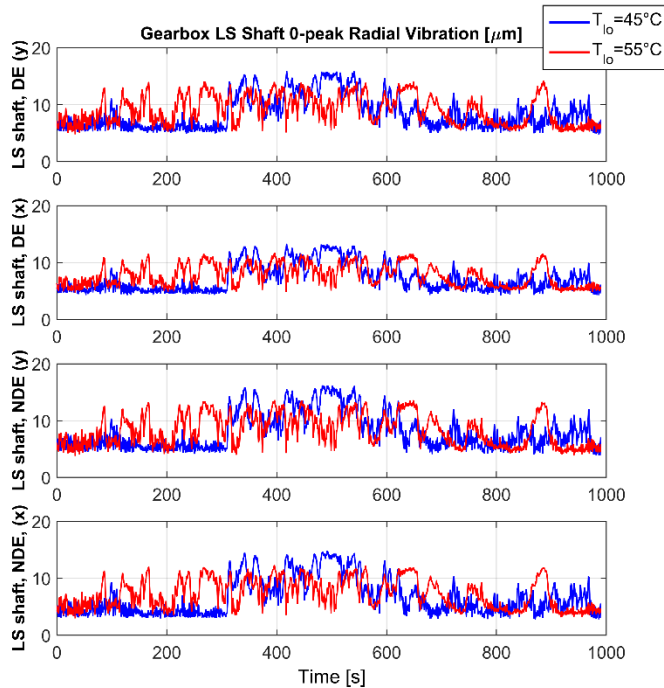

Figure 34 Gearbox LS shaft 0-peak lateral vibration trend at the 12f$_N$-12f$_M$ resonant point. Compressors load 0.29 [pu]
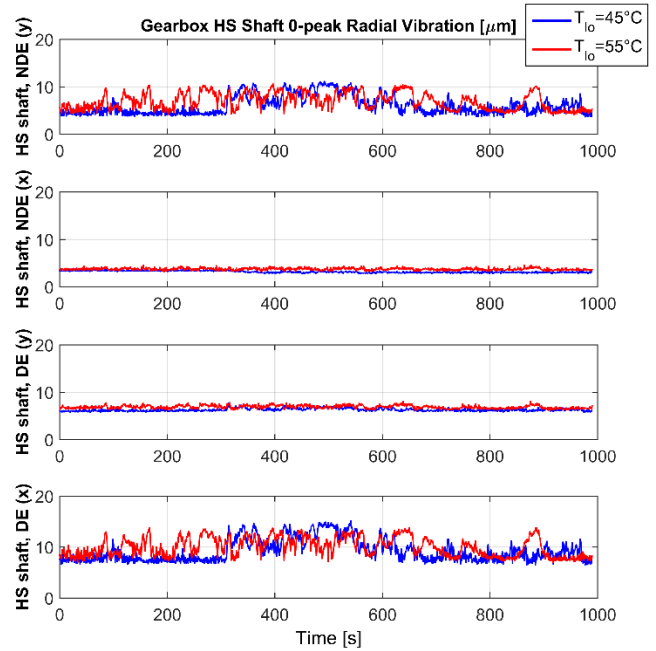

Figure 35 Gearbox HS shaft 0-peak lateral vibration trend at the 12f$_N$-12f$_M$ resonant point. Compressors load 0.29 [pu]
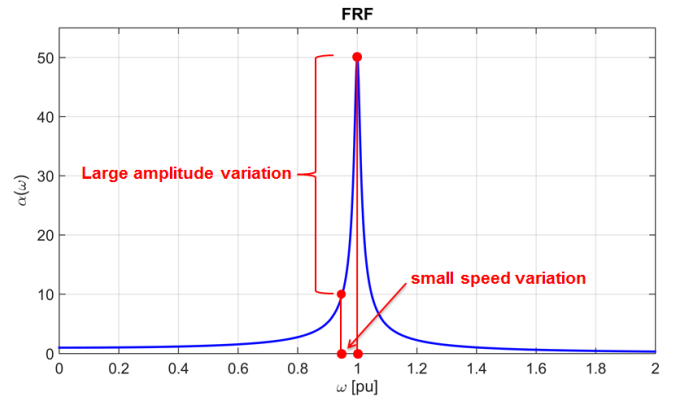

Figure 36 Frequency Response Function

Figure 37 Gearbox LS shaft, DE (x) Vibration Waterfall

at the $12f_N$-$12f_M$ resonant condition. Compressors load 0.29 [pu]. Lube oil temp. 45°C.

Figure 38 Gearbox LS shaft, DE (x) Vibration Waterfall at the $12f_N$-$12f_M$ resonant condition. Compressors load 0.29 [pu]. Lube oil temp. 55°C.

Figure 39 Gearbox HS shaft, DE (x) Vibration Waterfall at the $12f_N$-$12f_M$ resonant condition. Compressors load 0.29 [pu]. Lube oil temp. 45°C.

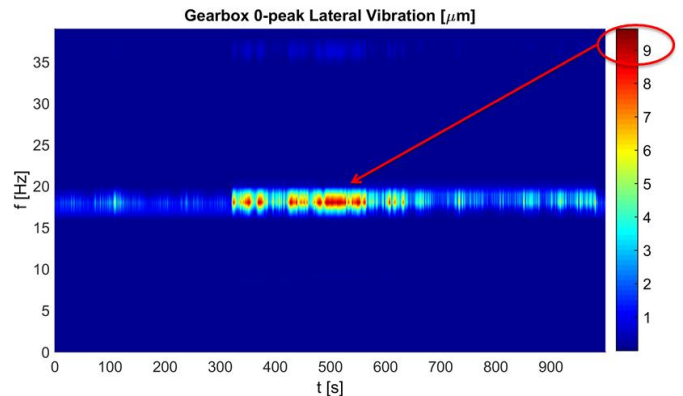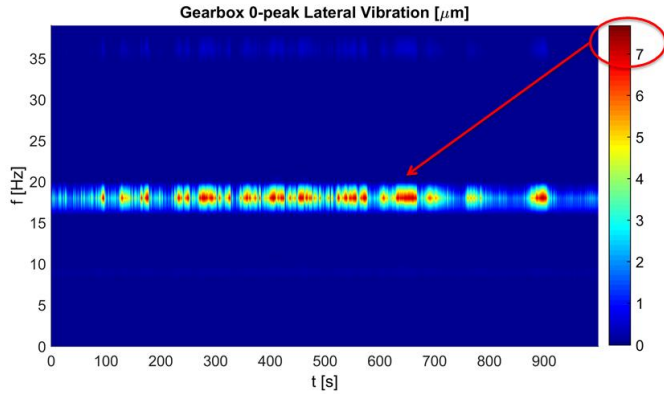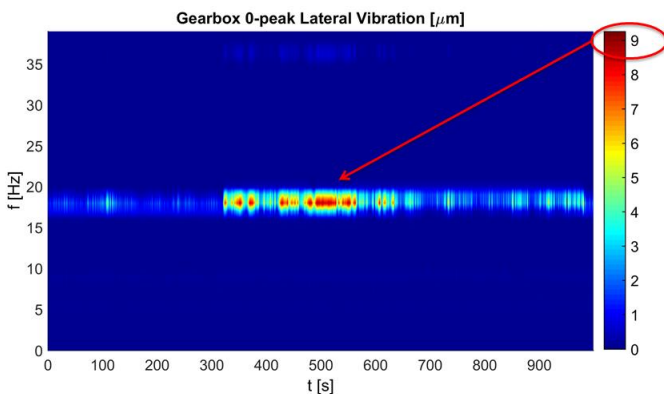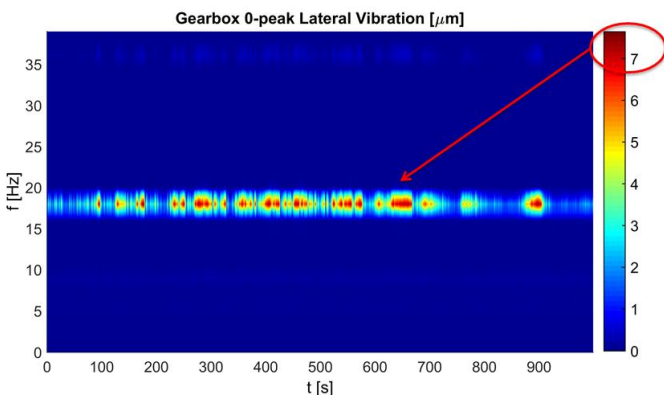**Figure 40 Gearbox HS shaft, DE (x) Vibration Waterfall at the $12f_N$-$12f_M$ resonant condition. Compressors load 0.29 [pu]. Lube oil temp. 55°C.**
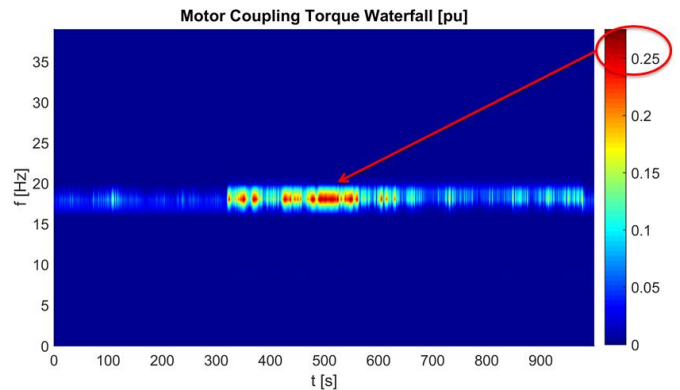
Figure 41 Motor Coupling Torque Waterfall at the $12f_N$-$12f_M$ resonant condition. Compressors load 0.29 [pu]. Lube oil temperature 45°C.
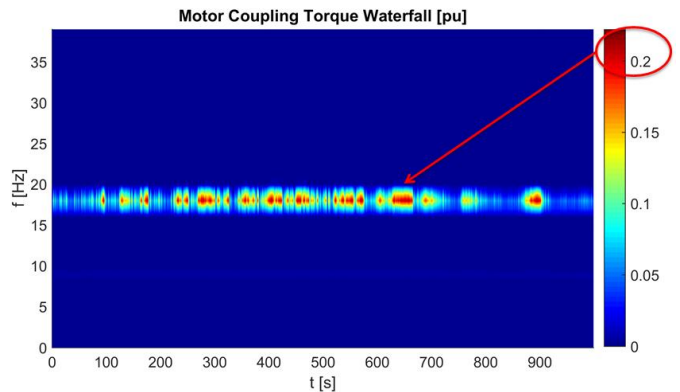
Figure 42 Motor Coupling Torque Waterfall at the $12f_N$-$12f_M$ resonant condition. Compressors load 0.29 [pu]. Lube oil temperature 55°C.

For sake of completeness, a summary of all the gearbox shaft vibrations at the frequency of the 1st TNF for the $12f_N - 12f_M$ intersection is provided in Table 5.

[0-peak µm]	LS shaft		HS shaft	
	45°C	**55°C**	**45°C**	**55°C**
DE (x)	9.6	7.5	9.1	7.5
DE (y)	11.9	10.0	1.2	1.4
NDE (x)	13.0	10.2	0.6	0.7
NDE (y)	12.9	10.7	8.3	7.0

Table 5 Gearbox max radial vibration at 1st TNF. Intersection with $12f_N$-$12f_M$ excitation. Compressors load 0.29 [pu].

Table 4 shows that the higher the lube oil temperature, the lower the amplification factor. The only maximum vibrations at 1st TNF which do not follow the above-mentioned trend are the HS shaft DE (y) and NDE (x), but their amplitudes are negligible with respect to the values reached by other probes at resonance conditions (see Figure 35). The first consequence of the lube oil inlet variation is the variation of gearbox shafts

lateral behavior due to the different bearing coefficients (stiffness and damping properties). It is to highlight that, the motor alternate input torque at the frequency of the 1st TNF basically remains constant for all the analyzed cases (amplitude about 0.01 [pu]), therefore the AF variation is due to the variation of output torque only.

With the decrease of temperature, the lube oil density is expected to increase. Considered the frequency of the phenomena, it looks like the most direct effect is a stiffening of the bearing as a bending constrain, resulting in an increase of the system vibration response, in terms of gear lateral vibration and train torsional vibration.

One can say that the kinematic interaction at the gear mesh, inducing the lateral vibration driven by the torsional one, looks like working also in the opposite direction. A torsional damping led by the lateral one, whose effect is a decrease of the torsional alternate torque measured by the torque-meter, appears.

Active Damping Control System Implementation

The Active Damping Control System was properly configured for the system under analysis with successful results. Figure 43 shows the results obtained in the worst torsional resonance condition ($6f_M - 6f_N$ (#3 of Table 1)).
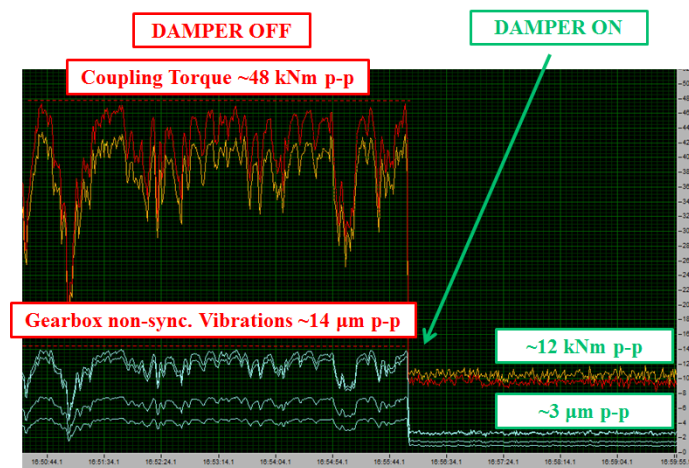

Figure 43 Motor Coupling Alternating Torque and Gearbox Lateral Vibrations at train 1st TNF

In particular, the red line represents the amplitude of the alternating torque at the train 1st TNF measured with the torque-meter system and the orange line the corresponding measurement with the strain gauges installed on the motor coupling. The light blue lines represents the amplitude of gearbox lateral vibrations at the train 1st TNF.

The active damping system has been able to reduce both the torsional vibrations and gearbox sub-synchronous vibrations by a factor of about 4, meeting all the demanding vibrations requirements for the string test. The system has been also successfully tested in transient condition, i.e. following a slow

speed ramp (0.5 rpm/s) across the torsional resonances within the operating speed range and with a fast speed ramp (10 rpm/s), as shown in Figure 44.
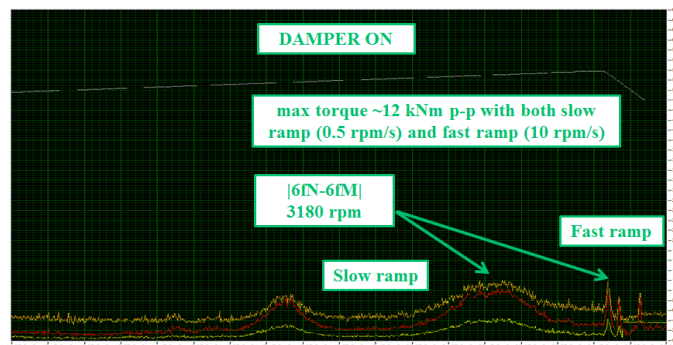

Figure 44 Motor Coupling Alternating Torque during Slow and Fast Speed Ramps

CONCLUSIONS

The use of Variable Speed Drive Systems as drivers for gas compression applications in the Oil & Gas industry is nowadays essential. These VSDSs allow a wide operating speed ranges and excellent reliability. Particular attention must be paid to the torsional behavior of VSDS-driven compressor shaft lines. In this paper, a comprehensive analysis of the key systems and parameters affecting the torsional modal response of a geared Load Commutated Inverter (LCI) driven motor-compressor is provided.

First, it is shown how important is the understanding of the train torsional mode shapes to identify the only ones of concern for a specific shaft line. Practically, those with negligible normalized amplitude in correspondence of the motor windings sections will not be able to be excited by any pulsating torque coming from the motor.

It is also shown how the knowledge of LCI drive working principles and control aspects are fundamental to properly identify the key parameters to be adjusted in order to minimize the torsional responses of the train. An even more effective solution towards this goal is active electrical damping, which has been implemented through the addition of a dedicated controller that commands the VSDS (of any kind in principle) to generate a torque variation that counteracts the torsional ones of interest. The main concepts related to the torsional excitation mechanism of a LCI fed synchronous motor are presented, and the closed-loop torsional interaction phenomena fully described.

For LCI VSDSs, the DC link current regulator has been identified as the most important control loop affecting these interactions. A thorough analysis of the related open loop and sensitivity transfer functions allowed defining the optimum tuning of the proportional gain of the DC current PI regulator as trade-off between the control stability and the capability to reject a disturbance inside the loop bandwidth. This allowed to

minimize the resulting motor pulsating torque occurring during a torsional resonance condition.

A method for measuring the actual torsional modal damping due to mechanical effects only is presented from the calculation of the log-dec (amplitude exponential) decay of a torsional measurement after a trip, showing an amplification factor of about 150. The modal amplification factor during several resonance conditions was also measured, showing how an optimized closed-loop behavior leads to a significant increasing of the overall modal damping, including both mechanical and electrical effects. The ensuing AF values are in the range of 50-70 for operation at nominal temperature of the lube oil at the bearings inlet. A sensitivity analysis of the AF during resonance conditions with different loads and lube oil temperature is presented.

It is shown that the higher the load, the lower the amplification factor. This can be addressed both to a load effect on the gearbox journal bearings (considering a coupling between torsional and lateral dynamics) and, more in general, to the resistant load acting in opposition to the shaft line twisting.

Besides, the higher the lube oil temperature, the lower the amplification factor. A torsional damping led by the lateral one was observed: the kinematic interaction at the gear mesh, inducing the lateral vibration driven by the torsional one, dually acts so that the torsional alternate torque measured by the torque-meter decreases in reason of lateral damping.

This analysis enhanced the complexity of the torsional-to-lateral dynamics behavior effect on the system modal response, thus is not practical to make design changes on gearbox bearings to meet demanding vibrations requirements.

In conclusion, the importance of a thorough understanding of electro-mechanical torsional interaction phenomena for geared LCI drive motor-compressors is emphasized: proper analysis during the engineering phase can, in fact, avoid equipment unnecessary oversizing and allow significant time reduction in performing train string tests and commissioning activities.

When the VFD control tuning optimization is still not sufficient to keep the torsional and gearbox lateral vibration amplitudes within the admissible limits, an active torsional damping system could be implemented, as successfully demonstrated in this paper. Experimental results from a real string test have been presented, showing the great effectiveness of the electrical active damping performed by a dedicated controller sending proper small corrective torque signals to the VSDS.

NOMENCLATURE

Variables

$[J]$	polar mass moments inertia matrix (full)
$[D]$	torsional damping matrix (full)
$[K]$	torsional stiffness matrix (full)

$\underline{\vartheta}$	angular d.o.f.s vector
$\underline{T}$	external torques vector
$[\Phi]$	matrix collecting torsional eigenvectors by columns
$\underline{q}$	modal d.o.f.s vector
$\underline{\varphi}^{(i)}$	i^{th} torsional modal shape (vector)
$[J_{mod}]$	modal polar mass moments inertia matrix (diagonal)
$[D_{mod}]$	modal torsional damping matrix (diagonal)
$[K_{mod}]$	modal torsional stiffness matrix (diagonal)
$\underline{T}_{mod}$	projections of external torque on the modal shapes (vector)
$D_{mod,i}$	diagonal i^{th} element of $[D_{mod}]$ (scalar)
$J_{mod,i}$	diagonal i^{th} element of $[J_{mod}]$ (scalar)
ω_i	i^{th} torsional critical speed
ξ_i	i^{th} modal torsional damping coefficient
f_M	motor frequency
f_N	network frequency
T_{EM}	actual motor air gap torque
$T_{mod\ 2}^{EM}$	scalar projection of T_{EM} on $\underline{\varphi}^{(1)}$
$T_{mod\ 2}^{EM}$	scalar projection of T_{EM} on $\underline{\varphi}^{(2)}$
$\varphi_{EM}^{(1)}$	scalar component corresponding to EM windings section of vector $\underline{\varphi}^{(1)}$
$\varphi_{EM}^{(2)}$	scalar component corresponding to EM windings section of vector $\underline{\varphi}^{(2)}$
$v_{DC,rect}$	rectifier side DC voltage
L	*DC link indurance*
i_{DC}	DC link current
$v_{DC,inv}$	inverter side DC voltage
$G(s)$	open loop transfer function
$G_{PI}(s)$	PI transfer function
$G_d(s)$	converter delay transfer function
$G_L(s)$	DC link inductance transfer function
k_p	proportional gain
k_i	integrative gain
τ	delay introduced by the converter
f_{line}	rectifier input voltage frequency
M_{ph}	phase margin
$S(s)$	Sensitivity function
AF_{test}	actual system amplification factor
AF_{DP}	amplification factor coming from internal design practice
ϕ_{1TNF}	contribution of the first modal shape to resonance response at coupling when input at EM
$T_{EM,test}$	$T_{EM,cmp} = T_{EM}$, measured alternate motor air gap torque also used for the computation ($T_{EM,test} = T_{EM,cmp} = T_{EM}$)
$T_{MC,test}$	actual motor coupling alternate torque
$T_{MC,cmp}$	Computed motor coupling alternate torque

Abbreviations

AC	Alternate Current

AF	Amplification Factor
CC	Centrifugal Compressor
CT	Current Transformer
DC	Direct Current
DE	Drive End
d.o.f.	degree of freedom
EM	Electrical motor
FRF	Frequency Response Function
HS	High Speed
LCI	Load Commutated Driver
LS	Low Speed
MCS	Maximum Continuous Speed
MOS	Minimum Operating Speed
NDE	Non Drive End
pu	per unit
SM	Synchronous Motor
TNF	Torsional Natural Frequency
VFD	Variable Frequency Drive
VSDS	Variable Speed Driver System
VT	Voltage Transformer

REFERENCES

[1] Mastroddi F. et al, 2015, *On the Modal Decoupling of Linear Mechanical Systems with Frequency-Dependent Viscoelastic Behavior*, Mechanical Systems and Signal Processing, Elsevier

[2] Naldi L. et al., 2011, *New Approach to Torsional Vibration Monitoring*, Proceedings of the 40th Turbomachinery Symposium, Turbomachinery Laboratory, Texas A&M University, College Station, Texas

[3] Del Puglia S. et al., 2010, *Torsional Interaction Optimization in a LNG Train with a Load Commutated Inverter*, Proceedings of the 8th IFToMM International Conference on Rotordynamics, KIST, Seoul, Korea

[4] Schramm S. H., 2010, *Damping of Torsional Interaction Effects in Power Systems*, Ph.D. thesis
https://mediatum.ub.tum.de/doc/957490/957490.pdf

[5] Ogata K., 2010, *Modern Control Engineering*, Prentice Hall

[6] Rotondo P. et al., 2009, *Combined Torsional and Electromechanical Analysis of an LNG Compressor Train With Variable Speed Drive System*, Proceedings of the 38th Turbomachinery Symposium, Turbomachinery Laboratory, Texas A&M University, College Station, Texas

[7] Sihler C. et al., 2009, *Torsional Mode Damping for Electrically Driven Gas Compression Trains in Extended Variable Speed Operation*, Proceedings of the 38th Turbomachinery Symposium, Turbomachinery Laboratory, Texas A&M University, College Station, Texas

[8] Bose B. K.., 2001, *Modern Power Electronics and AC Drives*, Prentice Hall

[9] Corbo M. et al., 1996, *Practical Guidelines against Torsional Vibration*, Proceedings of the 25th Turbomachinery Symposium, Turbomachinery Laboratory, Texas A&M University, College Station, Texas

[10] Inman D.J., 1996, *Engineering Vibration,* Prentice Hall

ACKNOWLEDGEMENTS